Chemical Engineering Journal 439 (2022) 135783

Contents lists available at ScienceDirect

Chemical Engineering Journal

journal homepage: www.elsevier.com/locate/cej

Mechanistic modelling of solar disinfection (SODIS) kinetics of *Escherichia coli,* enhanced with H_2O_2 – Part 2: Shine on you, crazy peroxide

Ángela García-Gil [a], Ling Feng [b], José Moreno-SanSegundo [a], Stefanos Giannakis [c,*], César Pulgarín [d,e], Javier Marugán [a,*]

[a] Department of Chemical and Environmental Technology (ESCET), Universidad Rey Juan Carlos, C/ Tulipán s/n, 28933 Móstoles, Madrid, Spain
[b] School of Ecology and Environment, Inner Mongolia University, University W. Road, 010021, Hohhot, Inner Mongolia, PR China
[c] Universidad Politécnica de Madrid (UPM), E.T.S. de Ingenieros de Caminos, Canales y Puertos, Departamento de Ingeniería Civil: Hidráulica, Energía y Medio Ambiente, Unidad docente Ingeniería Sanitaria, c/ Profesor Aranguren, s/n, Madrid ES-28040, Spain
[d] School of Basic Sciences (SB), Institute of Chemical Science and Engineering (ISIC), Group of Advanced Oxidation Processes (GPAO), École Polytechnique Fédérale de Lausanne (EPFL), Station 6, CH-1015 Lausanne, Switzerland
[e] Colombian Academy of Exact, Physical and Natural Sciences, Carrera 28 A No. 39A-63, Bogotá, Colombia

ARTICLE INFO

Keywords:
Multiple target – multiple hit
Light-heat synergy
Disinfection modelling
solar/H_2O_2
intracellular photo-Fenton

ABSTRACT

In this second part of the development of a mechanistic kinetic model of the solar inactivation of *E. coli* enhanced with hydrogen peroxide, we evaluate the mechanisms based on photonic inactivation and integrate them into the kinetic model of the dark process developed in Part 1. The direct photonic inactivation was modelled using a series-event model based on the accumulation of damage by photons and it was coupled with the model used in Part 1 for modelling the damage caused by radicals using a *multiple target – multiple hit* model, including recovery constant to define the ability of cells to face the specific photonic damage. Catalase and superoxide dismutase inactivation, the intracellular photo-Fenton reaction, and the overproduction of $O_2^{\bullet-}$ in the NADH/NAD^+ cycle under solar light were included in the model. Finally, the synergistic effect of the photonic damage with thermal inactivation was included in the kinetic constant of the series-event expression in terms of an Arrhenius equation. The kinetic parameters were obtained by model regression using experimental data at different temperatures, solar radiation, as well as initial cellular and H_2O_2 concentrations. Our model predictions can accurately describe the experimental data of the SODIS process enhanced with H_2O_2, thus being very useful to estimate disinfection profiles and inactivation routes at different irradiance conditions, water temperature and H_2O_2 concentration. Finally, an integrated mechanism of *E. coli* inactivation under the SODIS/H_2O_2 process is provided.

1. Introduction

Over the years, SODIS has proved its effectiveness in the inactivation of various microorganisms, such as bacteria, viruses, and protozoa [1–3]. Depending on the microorganism, solar inactivation can be achieved by three types of mechanisms at varying rates: i) direct endogenous damage, ii) indirect endogenous damage, and iii) indirect exogenous damage [2,4]. Endogenous damage (i and ii) refers to internal cell processes. Direct damage (i) is produced by absorption of radiation by some constituents of the pathogens (e.g., nucleic acid). In contrast, indirect damage (ii) is caused by attacks to the microorganism elements by photo-produced reactive intermediates (PPRIs) such as hydroxyl ($HO^{\bullet}$) and superoxide ($O_2^{\bullet-}$) radicals, hydroperoxyl radical ($HO_2^{\bullet}$), singlet oxygen ($^1O_2$), etc. which have been generated by photosensitisers and other chemical processes activated by solar photons. If the water contains suitable absorbing species, these PPRIs can also be produced outside the cells, hence this process is categorised as exogenous (indirect) damage (iii) [5].

Although SODIS has been systematically applied for almost three decades, a complete consensus on the relevant mechanisms leading to bacterial inactivation has not been reached yet. Regarding the endogenous damage, both mechanisms happen in the cell, as bacteria are complex microorganisms and contain several absorbing components, such as DNA and enzymes that directly get altered by light, or substances that can act as photosensitisers generating PPRIs [6,7]. For example, bacteria are vulnerable to direct photoinactivation since they have a

* Corresponding authors.
E-mail addresses: stefanos.giannakis@upm.es (S. Giannakis), javier.marugan@urjc.es (J. Marugán).

https://doi.org/10.1016/j.cej.2022.135783
Received 14 January 2022; Received in revised form 9 March 2022; Accepted 11 March 2022
Available online 15 March 2022

DNA genome that absorbs UVB solar radiation, while the presence of the porphyrin family of compounds has been considered a source of photosensitisation [8,9]. In addition to the aforementioned mechanisms, bacteria also generate PPRI during cell metabolism. Radicals randomly attack several targets producing cell damage. Under solar UV illumination, DNA photon absorption leads to its modification [10], the internal photo-Fenton process occurs [11], enzymes are deactivated [12], and the production of $O_2^{\bullet-}$ increases [13].

However, bacteria have mechanisms able to repair photodamages and damages caused by radical attacks, being often able to recover and regrow in darkness after light exposure [6,14–18]. Hence, numerous investigations have proposed ways to properly inactivate microorganisms by enhanced versions of SODIS with additives or photocatalysts, ensuring the absence of regrowth and rendering SODIS-treated water safer [19–21]. This phenomenon can be diminished by adding H_2O_2 to the water matrix to increase the bacteria inactivation, plus with a more permanent effect [22,23]. Generally, two different inactivation kinetic paths were found when H_2O_2 was added to water inoculated with *E. coli* [24]. *Mode-one killing* is related to internal damage produced by radicals' attacks, and it reaches its maximum around 1–2 mM H_2O_2 externally added concentration. For concentrations higher than 10 mM, *mode-two killing* mainly acts, directly leading to external cell wall damages. Between 2 and 10 mM, an intervening zone of partial resistance is observed. In addition, during water exposure to the sun, the water temperature can warm up to 50 °C. Hence, apart from the bacterial thermal inactivation caused by the denaturalisation of proteins and molecules that form cells [2], a synergistic effect between UV radiation and temperature on bacterial inactivation has been found [25–28]. Thermal action has a wider effect on the cell and a more permanent action against bacteria; it has been found critical to maintaining a regrowth-free matrix [29,30].

This highly desirable synergy between light and temperature has been the focal point of several investigations, jointly or in studying its constituents. More specifically, several efforts have been carried out to develop kinetic models to describe the inactivation pathways and accurately predict required exposure times to ensure the production of safe drinking water. Recent investigations incorporate significant advances; Uhl *et al.* [31], proposed a kinetic model to estimate and understand the internal pathways of bacteria when they are exposed to an H_2O_2-rich water matrix, albeit in the absence of light. Other works presented strides in solar involvement accounting for simultaneous thermal inactivation and photoinactivation [32] or the spectral distribution of radiation [33]. Also, a few examples of mechanistic models that involve the description of the intracellular inactivation pathways have been proposed to understand and predict inactivation times outside experimental set-up and studied operational conditions. Castro-Alférez *et al.*[34] developed a kinetic model that accounts for the internal balance of species that play an important role in the SODIS inactivation. Also, they used the Arrhenius equation approach to consider the thermal inactivation and the T-UV synergistic effect [27].

However, to the best of our knowledge, there is no mechanistic kinetic model available that describes both sets of routes and the effects of the joint action of light and temperature in a combined manner. Hence, based on the kinetic model that describes the mechanisms of cell inactivation under dark conditions developed in the first part of this manuscript, this work presents a holistic, rigorous mechanistic model of the SODIS process enhanced with H_2O_2 addition. The application of the model predictions allows the calculation of the time needed to provide safe drinking water, considering *E. coli* as a model bacterial pathogen one of the most used model microorganisms of faecal contamination [35], and sheds light in the tangled synergistic action modes involved. Ultimately, based on the results obtained in the dark with H_2O_2 and the modifications/added routes under solar light, an integrated bacterial inactivation mechanism is proposed.

2. Materials and methods

2.1. Chemicals and reagents

The chemicals used in the tests were all reagent grade or above. The aqueous H_2O_2 stock solution was prepared fresh, using Sigma-Aldrich Perdrogen^{TM} (30% w/w). Other reagents include plate count agar (PCA), Titanium (IV) Oxysulfate ($TiOSO_4$, 1.9–2.1%), which were all purchased from Sigma-Aldrich (Switzerland). All solutions used in this research were prepared prior to experimentation using ultrapure water (MilliQ, 18.2 MΩ cm).

2.2. Bacterial strain and growth protocol

The model bacterium used in this study, the wild-type *E. coli* K12, was acquired from DSMZ, Germany (Deutsche Sammlung von Mikroorganismen und Zellkulturen, Catalogue No. 498) in lyophilised powder form, reactivated by the supplier's protocol. Its propagation and growth followed previously reported protocols [36]. Briefly, in order to obtain a 10^9 CFU/mL stationary phase culture, a colony was dispersed in LB broth and grown overnight (>14 h), to an OD_{600} within the 3.5–5.5 range (shaking incubation set at 180 rpm, temperature: 37 ℃, in the dark).

2.3. Inactivation processes

The solar and solar/H_2O_2 experiments were performed using a SUNTEST CPS solar simulator from Hanau as a light source, employing a 1500-W, air-cooled xenon lamp. The simulator was equipped with an uncoated quartz glass light tube and cut-off filters for UVC (>290 nm) and IR wavelengths. The emission spectrum of this lamp matches satisfactorily with the solar spectrum at the Earth's surface in the UV range [37]. The selected solar radiation intensities applied in this research were set and calibrated frequently by a radiometer/pyranometer couple (CUV3/CM6b, Kipp and Zonen, Delft, Holland). The validation sets were monitored by a PCE-34 UV radiometer (PCE Iberica, Spain). The irradiance was measured at the water surface, and due to the low absorbance of the medium, it was assumed constant for the whole volume.

The tests were carried out in an open, 700-mL water-jacketed glass reactor with an irradiated surface of 0.0143 m^2. The solution was spiked with the 10^9 CFU/mL *E.* coli working bacteria solution, leading to a desired initial bacterial concentration depending on the test (10^4, 10^5, 10^6 and 10^7 CFU/mL). The bacterial solution was mixed 10 min in the absence of light, then a sample was plated to obtain the initial bacterial concentration (t = 0 min). A recirculating water bath (Julabo F25, Germany) was used to maintain a constant temperature within the reactors according to the desired experimental conditions (20, 30, 40, and 50 ℃). A magnetic bar was used to obtain a constant stirring speed of 350 rpm. H_2O_2 was added from a stock solution (final concentration: 0, 5, 10, 30, and 50 ppm). Finally, the xenon lamp was turned on, marking the beginning of the experiment.

2.4. Analytical measurements

2.4.1. Bacterial enumeration

The spread plate method for bacterial quantification was used, as previously reported [38]. Every dilution was plated in duplicates, and at least two consecutive dilutions were plated for each experiment.

3. Development of the mechanistic model.

This section describes the mechanistic modelling of the solar/H_2O_2 and solar/thermal *E. coli* inactivation, including the assumptions, parameters, and boundary conditions for the development of the kinetic model. The modelling of the solar *E. coli* inactivation was developed

Table 1
Mechanisms of the cell's respiration pathways and bacterial inactivation routes by radical's damage and thermal effect. In bold: reactions activated by light and kinetic parameters estimated in this work. Values of kinetic parameters without a reference were estimated in Part 1 of the present work.

R.1	$O_2^{\bullet-}$ generation during cell respiration	$O_2 + e^- \xrightarrow{NADH} O_2^{\bullet-}$	$r_1 = k_1^{'}[NADH] = k_1$	$k_1 = 5.4{\cdot}10^{-6} M{\cdot}s^{-1}$ [39]
R.12	**$O_2^{\bullet-}$ generation under light**	$\boldsymbol{NADH + O_2 \xrightarrow{h\nu} O_2^{\bullet-} + NAD^+ + H^+ + e^-}$	$\boldsymbol{r_{12} = k_{12}{\cdot}I{\cdot}[NADH]}$	$\boldsymbol{k_{12}(m^2{\cdot}J^{-1})}$
R.2	$O_2^{\bullet-}$ scavenging by SOD	$O_2^- + H^+ + SOD \rightarrow \frac{1}{2}H_2O_2 + \frac{1}{2}O_2$	$r_2 = k_2{\cdot}[O_2^-][SOD]$	$k_2 = 10^9 M^{-1}s^{-1}$ [40]
R.13	**SOD deactivation**	$\boldsymbol{SOD \xrightarrow{h\nu} SOD_i}$	$\boldsymbol{r_{13} = k_{13}{\cdot}I{\cdot}[SOD]}$	$\boldsymbol{k_{13}(m^2{\cdot}J^{-1})}$
R.3	H_2O_2 scavenging by CAT	$H_2O_2 + CAT \rightarrow \frac{1}{2}O_2 + H_2O$	$r_3 = k_3[H_2O_2][CAT]$	$k_3 = 9{\cdot}10^5 M^{-1}s^{-1}$ [34]
R.14	**CAT deactivation**	$\boldsymbol{CAT \xrightarrow{h\nu} CAT_i}$	$\boldsymbol{r_{14} = k_{14}{\cdot}I{\cdot}[CAT]}$	$\boldsymbol{k_{14}(m^2{\cdot}J^{-1})}$
R.4	Internal Fenton process	$Fe^{2+} + H_2O_2 \rightarrow Fe^{3+} + HO^- + HO^{\cdot}$	$r_4 = k_4[Fe^{2+}][H_2O_2]$	$k_{04} = 8.21{\cdot}10^{11}\ M^{-1}s^{-1},\ E_{a4} = 4.9{\cdot}10^4\ J{\cdot}mol^{-1}$
R.5	Internal Fenton-like process	$Fe^{3+} + Donor^{red} \rightarrow Fe^{2+} + Donor^{ox}$	$r_5 = k_5[Fe^{3+}]$	$k_5 = 8.433{\cdot}10^{-2}s^{-1}$
R.15	**Internal Photo-Fenton**	$\boldsymbol{Fe^{3+} + H_2O \xrightarrow{h\nu} Fe^{2+} + H^+ + HO^{\cdot}}$	$\boldsymbol{r_{15} = k_{15}{\cdot}I{\cdot}[Fe^{3+}]}$	$\boldsymbol{k_{15} = 3.92{\cdot}10^{-5} m^2{\cdot}J^{-1}}$
R.6	Radical self-scavenging	$H_2O_2 + HO^{\cdot} \rightarrow O_2^{\cdot-} + H_2O + H^+$	$r_6 = k_6[H_2O_2][HO^{\cdot}]$	$k_6 = 2.7{\cdot}10^7 M^{-1}s^{-1}$ [41]
R.7	$O_2^{\bullet-}$ disproportionation	$2O_2^{\cdot-} + 2H^+ \rightarrow H_2O_2 + O_2$	$r_7 = k_7[O_2^{\cdot-}]^2$	$k_7 = 33.04\ M^{-1}s^{-1}$ [42]
R.8	$HO^{\bullet}$ recombination	$2HO^{\cdot} \rightarrow H_2O_2$	$r_8 = k_8[HO^{\cdot}]^2$	$k_8 = 4.6{\cdot}10^9 M^{-1}s^{-1}$ [43]
R.9	Bacterial damage mediated by $O_2^{\bullet-}$	$B_i + O_2^{\cdot-} \rightarrow B_{i+1}$	$r_9 = k_9[O_2^{\cdot-}][B_i]$	$n = 27$ [44] $\quad k_9 = 33.1\ M^{-1}s^{-1}$
R.10	Bacterial damage mediated by $HO^{\bullet}$	$B_i + HO^{\cdot} \rightarrow B_{i+1}$	$r_{10} = k_{10}[HO^{\cdot}][B_i]$	$k_{10} = 5{\cdot}10^{-5} M^{-1}s^{-1}$
				$k_{R-ROS} = 10.8 s^{-1}$
R.11	Thermal inactivation	$B_v \xrightarrow{T} B_{inactivated}$	$r_{11} = k_{11}(T)[B_v]$	$k_{011} = 4.18{\cdot}10^{19}s^{-1},\ E_{a11} = 1.38{\cdot}10^5 J{\cdot}mol^{-1}$
R.16–1	**Direct DNA damage (at 20 °C)**	$\boldsymbol{B_v \xrightarrow{h\nu} B_j}$	$\boldsymbol{r_{16} = k_{16}(I)[B_j]}$	m = 5 [44]
				$\boldsymbol{k_{16}(m^2{\cdot}J^{-1})k_{R-RAD}(s^{-1})}$
R.16–2	**Direct DNA damage + T-UV synergy**	$\boldsymbol{B_v \xrightarrow{h\nu,T} B_j}$	$\boldsymbol{r_{16} = k_{16}(I,T)[B_j]}$	m = 5 [44] $k_{R-RAD} = 1.75{\cdot}10^{-3}s^{-1}$, $\boldsymbol{k_{016}(m^2{\cdot}J^{-1}),\ E_{a16}\left(J{\cdot}mol^{-1}\right)}$

considering the dark model of Part 1, which accounts for the main processes involved in the cell respiration: generation of radical species and defence mechanisms (Table 1: R.1-R.11) and the effect of the H_2O_2 presence in water on the cell inactivation (Table 2: R.A-R.D). Briefly, bacteria carry out cell respiration to generate energy, involving electron transport. A small portion of free electrons interact with oxygen to produce $O_2^{\bullet-}$ (R.1). This substance is scavenged by superoxide dismutase (SOD) enzymes (R.2), producing H_2O_2. The latter is scavenged by alkyl hydroperoxide reductase enzyme (Ahp) and catalases (CAT) enzymes (depending on the growth phase) (R.3), but also it can interact with internal iron by the Fenton reaction to generate $OH^{\bullet}$ (R.4). Meanwhile, ferrous iron is recycled into ferric iron (R.5). $O_2^{\bullet-}$ and $HO^{\bullet}$ can react with each other and with H_2O_2 (R.6, R.7 and R.8) but also indiscriminately attack several cell targets (R.9 and R.10). However, bacteria have their own defence mechanisms which repair damage caused by radical attacks (also R.9 and R.10). Furthermore, bacteria also can be thermally inactivated (R.11), whose role resulted in being predominant for temperatures above 50 °C, and insignificant for temperatures below 30 °C. For intermediate temperature, the contribution of radicals' damage and thermal inactivation on cell death was comparable. In addition, the model also includes the sinks of H_2O_2: decomposition (R.A), permeation into the cell (R.B), interaction with the cell membrane (R.C), and interaction with cell components and remaining debris from the dead cells (R.D), which are the main sink of ineffective consumption of the externally added H_2O_2.

Hence, the steps followed to model the inactivation kinetics of *E. coli* induced by the addition of H_2O_2 in the water matrix under solar illumination at different temperatures, given the developments of the corresponding dark experiments of Part 1 of the study, were: 1) the study of the direct and indirect photonic mechanisms carried out in bacteria and H_2O_2, and 2), the study of the radiation-temperature synergistic effect. Rigorous kinetic description of the photoactivated reactions requires the explicit inclusion of the photon absorption rate for each absorbing species in the model as follows (eq. (1)):

$$r_i = \phi_i(\lambda){\cdot}e_{a_i}(\lambda)d\lambda \tag{1}$$

where $\phi_i(\lambda)$ is the quantum yield (reacted species per photon), and $e_{a_i}(\lambda)$ is the spectral local volumetric rate of photon absorption (LVRPA). Both kinetic parameters depend on the wavelength. The value of absorbed energy by each species ($[i]$) is the integral of the product of incident radiation ($G(\lambda)$) by the specific absorption coefficient $\kappa_i(\lambda)$ along the wavelength range (eq. (2)).

$$e_{a_i} = \int_{\lambda} G(\lambda){\cdot}\kappa_i(\lambda)d\lambda{\cdot}[i] \tag{2}$$

Assuming that: i) ϕ_i can be considered constant in the UV solar range; ii) the irradiance at the water surface ($I(\lambda)$) can be considered as the average incident radiation of the total volume ($G(\lambda)$) due to the short optical path; iii) the product of multiplying ($G(\lambda)$) by $\kappa_i(\lambda)$ is constant since the spectral distribution of light does not vary in the used solar simulator, the photoactivated reaction rate can be rewritten as eq. (3):.

$$r_i = k_i{\cdot}I{\cdot}[i] \tag{3}$$

where the kinetic constant (k_i) acts as a second-order kinetic constant with respect to the irradiance at the surface and the concentration of the species. This assumption was applied for all the absorbing species considered in this work (NADH, SOD, CAT, iron, and DNA).

This model is rigorous enough to describe the intrinsic mechanisms that occur in bacteria in solar irradiated H_2O_2-rich water. However, a rigorous description of all involved biochemical routes is far from practical. Mechanistic models capture the fundamental steps of the global process and are considered as an optimal compromise between the basic description of the process and the simplicity of the model's requirements for engineering objectives [2]. The kinetic model in light conditions continues the work developed in the first part of the manuscript, whose reactions and kinetic parameters are summarised in

Table 2
Mechanism of the H_2O_2 decomposition and its consumption when added to water inoculated with *E. coli*.

R.A	H_2O_2 decomposition	$H_2O_{2_{ext}} \xrightarrow{T} \frac{1}{2}O_2 + H_2O$	$r_A = k_A[H_2O_{2ext}]$	$k_{0A} = 3.95{\cdot}10^2 s^{-1}$ $E_{aA} = 4.48{\cdot}10^4 J{\cdot}mol^{-1}$
R.B	H_2O_2 permeation	$H_2O_{2_{ext}} \rightarrow H_2O_2$	$r_B = k_B([H_2O_{2ext}] - [H_2O_2])$	$k_B = 70\ s^{-1}$ [45]
R.C	Membrane-H_2O_2 interaction	$H_2O_{2_{ext}} + B_v \rightarrow \frac{1}{2}O_2 + H_2O + B_v$	$r_C = k_C[B_v][H_2O_{2_{ext}}]$	$k_C = 2.04{\cdot}10^{10} M^{-1}s^{-1}$
R.D	MO killed cells-H_2O_2 interaction	$H_2O_{2_{ext}} + OM_{red} \xrightarrow{T} OM_{ox}$	$r_D = k_D[OM_{red}][H_2O_{2_{ext}}]$	$k_{0D} = 2.14{\cdot}10^7 M^{-1}s^{-1}$, $E_{aD} = 4.93{\cdot}10^4 J{\cdot}mol^{-1}$, $\zeta = 3.63{\cdot}10^{11}$

Tables 1 and 2. The kinetic steps taken into account in this Part 2 are briefly presented in bold in Table 1, namely the bacterial mechanisms involved in the photochemical processes and the synergistic effect of UV light with temperature. Afterwards, a detailed description of the mechanisms involved is provided to explain the fundamentals of each reaction. Since H_2O_2 did not show different behaviour under light conditions, no reactions were added in Table 2 (see next section).

3.1. H_2O_2 photonic mechanisms

As it was expected, the same results of the H_2O_2 decomposition in dark and illuminated conditions were obtained (data not shown). H_2O_2 does not present activation under solar light, and its decomposition is rather thermal driven. Therefore, the solar light did not cause any effect on the H_2O_2 dissolved in water, and no kinetic description was required.

3.2. Bacterial photonic mechanisms

Firstly, the mechanisms inflicted by indirect pathways were studied (R.12, R.13, R.14, and R.15). Secondly, the direct damage mechanism was evaluated (R.16).

3.2.1. ROS overproduction (R.12)

$O_2^{\bullet-}$ is a by-product of cell respiration since few of the free electrons generated in the redox cycle of the nicotinamide adenine dinucleotide enzyme (NAD^+/NADH) interact with oxygen. During the UV illumination, the redox cycle follows another pathway is introduced that depends on the NADH concentration and the UV light intensity, since NADH presents clear absorption peaks at 260 (not within our range of illumination or environmentally relevant) and 340 nm [46]. The route comprises the following steps: (i) NADH is promoted to an excited state (NADH*) and is quickly decomposed to $NADH^{\bullet+}$; (ii) $NADH^{\bullet+}$ forms an intermediate species ($NAD^{\bullet}$) that reduces O_2 to $O_2^{\bullet-}$ forming NAD^+; (iii) NAD^+ is reduced to initial NADH [46]:

i) $NADH \xrightarrow{h\nu} NADH^* \rightarrow NADH^{\cdot+} + e^- / \ r_{NADH^+} = \phi{\cdot}e_{a_{NADH}}$.

ii) $NADH^+ + O_2 \rightarrow NAD^+ + H^+ + O_2^{\cdot-} / r_{O_2^-} = k^{\cdot}{\cdot}O_2{\cdot}NADH^+$.

iii) $NAD^+ + H^+ + 2e^- \rightarrow NADH$.

These are the steps of the global reaction of $O_2^{\bullet-}$ production caused by solar light, which can be expressed as R.12. To the best of our knowledge, the kinetic constant (k_{12}) is unknown, being estimated in this work by a model regression.

3.2.2. ROS scavenging enzymes deactivation (R.13 and R.14)

Superoxide dismutases (the cytoplasmic SodA, SodB and the periplasmic SodC, hereon: SOD) are the main scavengers of the harmful $O_2^{\bullet-}$ but so far, there are no clear indications that SOD enzymes are photosensitive. Nevertheless, we base our hypothesis on the fact that a FeSOD enzyme in *Desulfovibrio gigas* has a broad absorption peak with a maximum at 280 nm and a small absorption band with a maximum at 470 nm and a shoulder around 600 nm, which is reported to be typical of FeSODs, like SodB of *E. coli*, one of the two cytoplasmic dismutases [47,48]. Here we consider the total dismutase activity as SOD, and this reaction can be expressed as R.13 in which, to our knowledge, the kinetic constant (k_{13}) is unknown and was estimated in this work by model regression. (Note: later we prove that their inactivation being x1000 slower than CAT makes them practically not degradable by light, *vide infra*).

Catalases (KatG or HPI, and KatE or HPII, hereon: CAT) are the enzymes able to scavenge H_2O_2 to avoid its conversion to more reactive radical forms. HPI is heat-labile, whereas HPII, the stationary phase catalase, is heat-stable [49]. However, we suggest that light can inactivate CAT, since heme-containing catalases present distinct absorption peaks within the solar range (404–406, 500–505 and 535–540 nm); for instance, (EC 1.11.1.6 catalase from *Desulfovibrio gigas* has two absorption peaks at 280 (with tail in our spectral region) and 405 nm [48]. We consider the total catalase activity of *E. coli* as CAT in this work [50–52], and this reaction can be expressed as R.14. To the best of our knowledge, the kinetic constant (k_{14}) is unknown, and it will be independently estimated in this work using reported data of the CAT inactivation with UV solar light. k_{14} was independently obtained using data reported in the literature: In a previous study, Castro-Alférez et al. [34] measured the CAT inactivation under constant values of UV solar irradiance (30 and 50 $W{\cdot}m^{-2}$). However, the second-order kinetic constant of the photoactivated reactions with regards to the species' concentration and incident radiation was not obtained. Since the incident radiation is constant during each experiment, the product of multiplying the kinetic constant by the irradiance is a new pseudo first-order kinetic constant we calculated, which was obtained by applying a linear fitting to the CAT concentration profiles.

3.2.3. Photo-Fenton reaction (R.15)

Fenton-like reactions happen inside the cell since free iron is involved in a redox cycle to scavenge H_2O_2 producing $HO^{\bullet}$ (dark reactions: R.4 and R.5). Under solar radiation, photo-Fenton-like reactions (R.15) produce additional $HO^{\bullet}$ as iron is activated with near-UV radiation up to 600 nm [53]. This reaction has a critical role in ferric reduction and hydroxyl radical generation, and its kinetic constant was estimated to R.15 as $k_{15} = 3.92{\cdot}10^{-5}\ m^2{\cdot}J^{-1}$ [44].

3.2.4. Direct DNA damage (R.16–1)

DNA directly absorbs photons, leading to various issues in its bases and ultimately cell death [10]. Photons in the UVB range (280–320 nm) contribute to (endogenous) direct damage since DNA absorption spectra extends up to 320 nm [54], while photons within the UVA region (320–400 nm) are involved in indirect reactions and will not be considered in this category (interested readers should refer to Giannakis *et al.*, [4]). As well as the kill mode of radicals, bacteria need the accumulation of damage caused by direct DNA absorption to cause the cell inactivation. The series-event kinetic model [55] considers that an event is a unit of damage, and m units of damage must be accumulated to kill the microbes. Thus, the inactivation process takes place through a series of inactivation levels (m), and the reaction rate of each level is a function of the kinetic constant (k_{16}), UV radiation intensity and bacterial

concentration at this stage. Since UV damage is targeted to specific molecules, bacteria have long developed recovery mechanisms to protect themselves from low levels of UVB radiation [6]. The recovery path can be expressed with a first-order kinetic reaction in which the rate depends on the kinetic constant (k_{R-RAD}) and the damaged bacteria concentration at level j. Therefore, in order to calculate the number of bacteria at level j ($1 \leq j \leq m$), it is necessary to account for the damaged organisms from the previous level (B_{j-1}) and the recovered organisms from the next level (B_{j+1}) as sources of organisms (positive terms), and the damaged and recovered organisms of the current level (B_j) as sinks of organisms (negative terms), respectively. This balance is represented by eq. (4):

$$\frac{dB_j}{dt} = k_{16}\cdot I\cdot B_{j-1} + k_{R-RAD}\cdot B_{j+1} - k_{16}\cdot I\cdot B_j - k_{R-RAD}\cdot B_j \quad (4)$$

Casado *et al.* [44] estimated a level of $m = 5$ when modelling the required number of levels of damage to directly inactivate *E. coli* by solar radiation. The same number of levels is assumed in this work. Our tests showed inactivation starting from the lowest irradiance (10.6 $W\cdot m^{-2}$). Thus, k_{16} and k_{R-RAD} were optimised by model regression.

3.3. Synergistic T-UV effect (R.16–2).

It has been proven that temperature and UV radiation produce a synergistic inactivation effect on microorganisms [25,56,57]. To account for this synergistic effect in the model, k_{16} from eq. (4) was redefined with the Arrhenius equation [32] (eq. (5)):

$$k_{16} = k_{016}\exp\left(\frac{-Ea_{16}}{RT}\right) \quad (5)$$

where k_{016} is the temperature-independent pre-exponential factor, Ea_{16} is the activation energy, R is the ideal gas constant, and T is the water temperature (K). The kinetic parameters of the synergistic model (k_{016}, Ea_{16}) were calculated carrying out the model regression with a new set of experiments at higher temperatures and considering the obtained value of k_{16} at 20 °C (293 K). For this purpose, the following condition (eq. (6)) was incorporated into the model:

$$k_{016} = k_{16}(293K) \Big/ \exp\left(\frac{-Ea_{16}}{R\cdot 293}\right) \quad (6)$$

3.4. Regression methodology

To solve the model, firstly, the photonic mechanism was assembled, including the light-inflicted damage and the underlying dark mechanisms from Part 1. To this end, R.12, R.13, R.14, and R.15 were independently incorporated into the dark model as four additional reactions. However, in order to add the inactivation due to the direct photonic damage (R.16–1/2), the balance of inactivated cells by radical attacks (R.9 and R.10) needed to be modified. In the SODIS process enhanced with H_2O_2, two stress sources must be accounted for: i) radicals' attack on DNA and cell elements, and ii) solar inactivation due to direct absorption by DNA. Both mechanisms are based on the accumulation of damage levels to inactivate the cell. But, if both mechanisms are considered as independent additive effects (incorporating the two series-event reactions independently), each cell could be considered as inactivated twice: once caused by radical's damage and another due to direct solar damage. At this point, the *multiple target – multiple hit* model was used, in which the model remembers the number of attacks of each type, avoiding the inactivation of the same cell by both routes. This model was developed by Casado *et al.* [44], and it is built with a 2-D matrix, one per stress source. The attack from each source moves the bacteria one step forward in its dimension, while each independent recovery path moves the bacteria one step back. Once the kinetic model was assembled, the normalised root mean square logarithmic error (NRMSLE) between predictions and experimental data of the *E. coli* inactivation profiles was minimised. The sequential quadratic programming (SQP) optimisation method from GNU Octave was used to minimise the objective error function. The system of differential equations was solved using explicit Euler. An independence analysis was carried out to achieve a value of the time step low enough.

The missing kinetic parameters were grouped in two categories: a) independent, or b) dependent on the T-UV synergy effect. In order to reduce the number of variables, two regression steps were defined.

a) ***T-UV independent parameters***: The first regression step considers k_{16} (R.16–1) at 20 °C and as constant. Experimental data of the *E. coli* inactivation profiles at 20 °C (temperature low enough to avoid the thermal and T-UV synergistic effect and consider k_{16} as constant) were used to estimate the kinetic parameters free of the influence of the synergistic effect:k_{12},k_{13},k_{16}, andk_{R-RAD}. For that, three sets of experiments were used: (1) different UV solar irradiances (10.6, 15.0, and 20.8 $W\cdot m^{-2}$) for an initial cell concentration of 10^6 $CFU\cdot mL^{-1}$ and initial H_2O_2 concentration of 0 and 50 ppm, (2) different bacterial initial concentration (10^4, 10^5, 10^6, and 10^7 $CFU\cdot mL^{-1}$) for an initial H_2O_2 concentration of 10 and 50 ppm at 15.0 $W\cdot m^{-2}$, and (3) different H_2O_2 initial concentrations (5, 10, 20, 30, and 50 ppm) for a cell initial concentration of 10^6 $CFU\cdot mL^{-1}$ at 15.0 $W\cdot m^{-2}$.

b) ***T-UV dependent parameters***: The second regression step considers that k_{16} (R.16–2) is defined as eq. (5) accounting for the restriction expressed in eq. (6). This regression uses experimental data of the *E. coli* inactivation profiles at 30, 40, and 50 °C to estimate the kinetic parameters involving the synergistic effect: k_{016},Ea_{16}. For that, two sets of experiments were used: (1) different UV solar irradiances (10.6, 15.0, and 20.8 $W\cdot m^{-2}$) at water temperatures of 50 °C and initial H_2O_2 concentrations of 10 and 50 ppm, and (2) different H_2O_2 initial concentrations (5, 10, 20, 30, and 50 ppm) at 15.0 $W\cdot m^{-2}$ and water temperatures of 30, 40 and 50 °C (10^6 $CFU\cdot mL^{-1}$ cell initial concentration for both sets).

4. Results and discussion

4.1. Catalase inactivation by solar light: k_{14}

The kinetic constant of the CAT photo-inactivation was estimated as $k_{14} = 2.74\cdot10^{-5}$ $m^2\cdot J^{-1}$ (R = 0.95). The fit between the predicted results and the experimental data provided by Castro-Alférez *et al.* [34] is shown in Fig. 1.

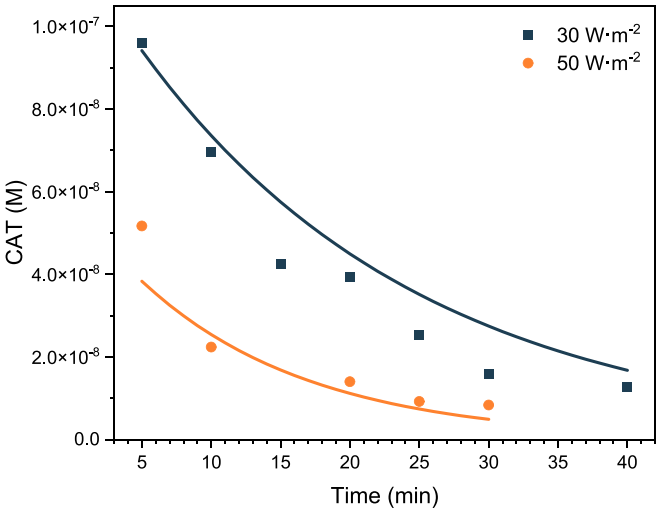

Fig. 1. Observed and predicted CAT concentration profiles under different conditions of solar UV irradiance at temperatures below 30 °C. Line: predicted data. Dots: experimental data (obtained from the literature [34]).

4.2. Direct photonic inactivation (no temperature effects)

For the calculation of the kinetic parameters of the photonic mechanisms, experiments performed at 20 °C were just used, and the values were estimated as $k_{12} = 1.07{\cdot}10^{-4}$ $m^2{\cdot}J^{-1}$, $k_{13} = 1.41{\cdot}10^{-7}$ $m^2{\cdot}J^{-1}$, $k_{16} = 2.23{\cdot}10^{-4}$ $m^2{\cdot}J^{-1}$, and $k_{R-RAD} = 1.75{\cdot}10^{-3}$ s^{-1} with an NRMSLE of 17.3%. The corresponding fitted curves are shown in Fig. 2**A-B**, Fig. 3**A**, and Fig. 4**A-B**.

Regarding the photo-inactivation of enzymes, the value of the kinetic constant for SOD is significantly lower than the value for CAT ($k_{13} = 1.41{\cdot}10^{-7} \ll k_{14} = 2.74{\cdot}10^{-5}$ $m^2{\cdot}J^{-1}$). SOD was found to be intrinsically more resistant to UVB light than CAT [58], and this is probably to the relevant absorption spectra: while CAT has an absorption peak at 405 nm, Fe-SOD has a small absorption band around 470 nm [47,48].

Despite the results in dark conditions in which the *E. coli* inactivation profiles resulted to be linear, all the inactivation curves under UV illumination (Fig. 2, Fig. 3, and Fig. 4) showed the characteristic curved shape of the series-event model. In this case, the low value of the photonic recovery constant ($k_{R-RAD} = 1.75{\cdot}10^{-3}$ s^{-1}), i.e., the rate describing the light-mediated repair mechanisms of the cell (related to the DNA damages), is not capable of straightening the curve. The number of radicals' attacks (m = 27) is 5.5 times higher than the number of damage levels by the direct photonic process, confirming the critical effect produced by photons in comparison with radicals. In contrast, the recovery constant for radical damage is much lower than the solar one, but it must also go through a higher number of levels to completely heal the bacteria, resulting again in higher potential damage produced by light. Bacteria are used to radical attacks due to cell respiration and not to photonic damage, thus, we suggest that this is the reason why bacteria are more sensitive to photonic damage than radicals' attacks.

As shown in Fig. 2**A-B** and Fig. 3**A**, the photonic damage, as well as the radical damage caused by H_2O_2 permeation into the cell, have important contributions in the cell inactivation at 20 °C.

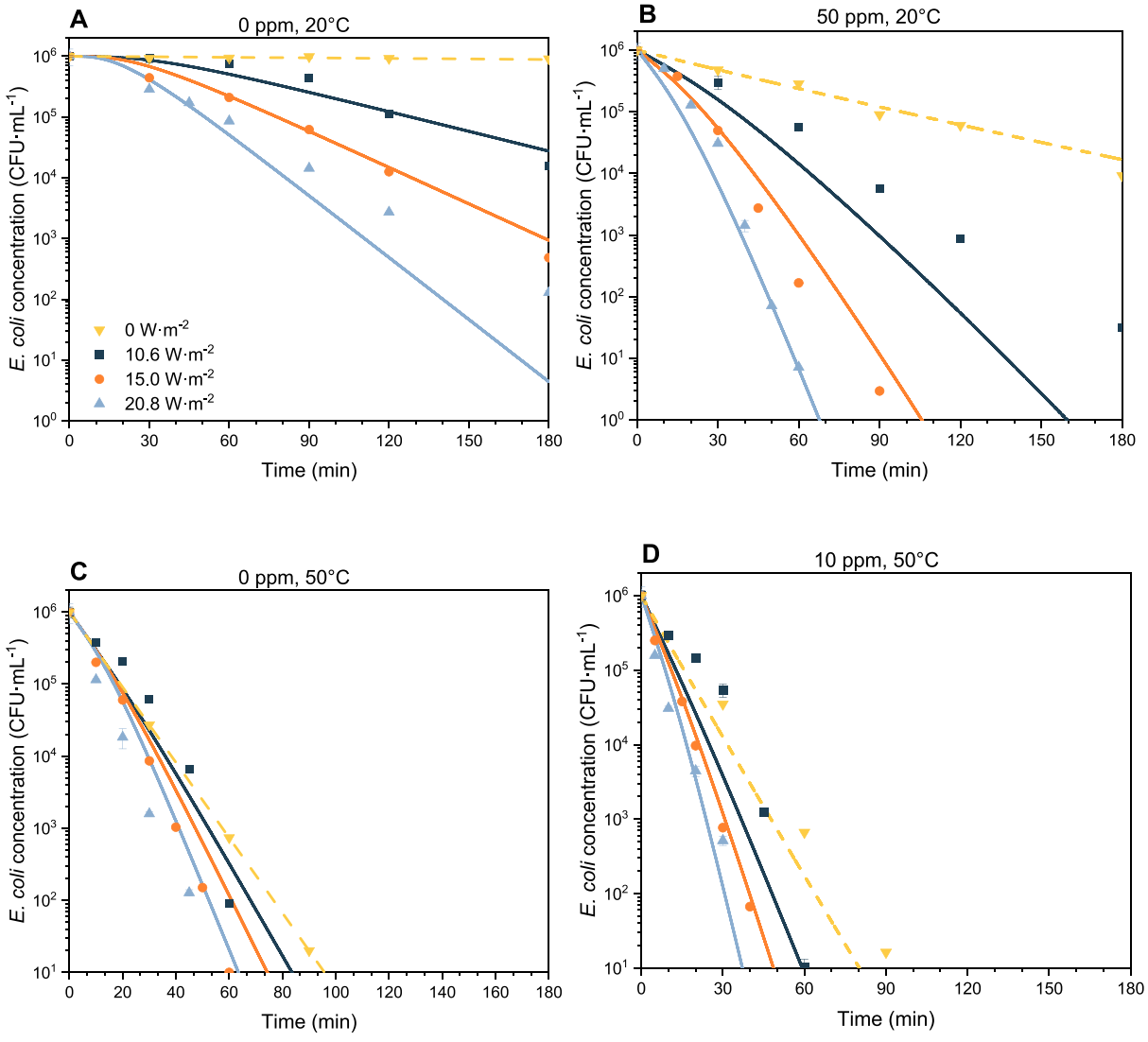

Fig. 2. Evolution of the *E. coli* concentration profiles depending on the UV irradiance at different conditions of initial H_2O_2 external concentration and water temperature. Line: predicted data. Dots: experimental data. A) 0 ppm H_2O_2 and 20 °C, B) 50 ppm H_2O_2 and 20 °C, C) 0 ppm H_2O_2 and 50 °C, and D) 10 ppm H_2O_2 and 50 °C.

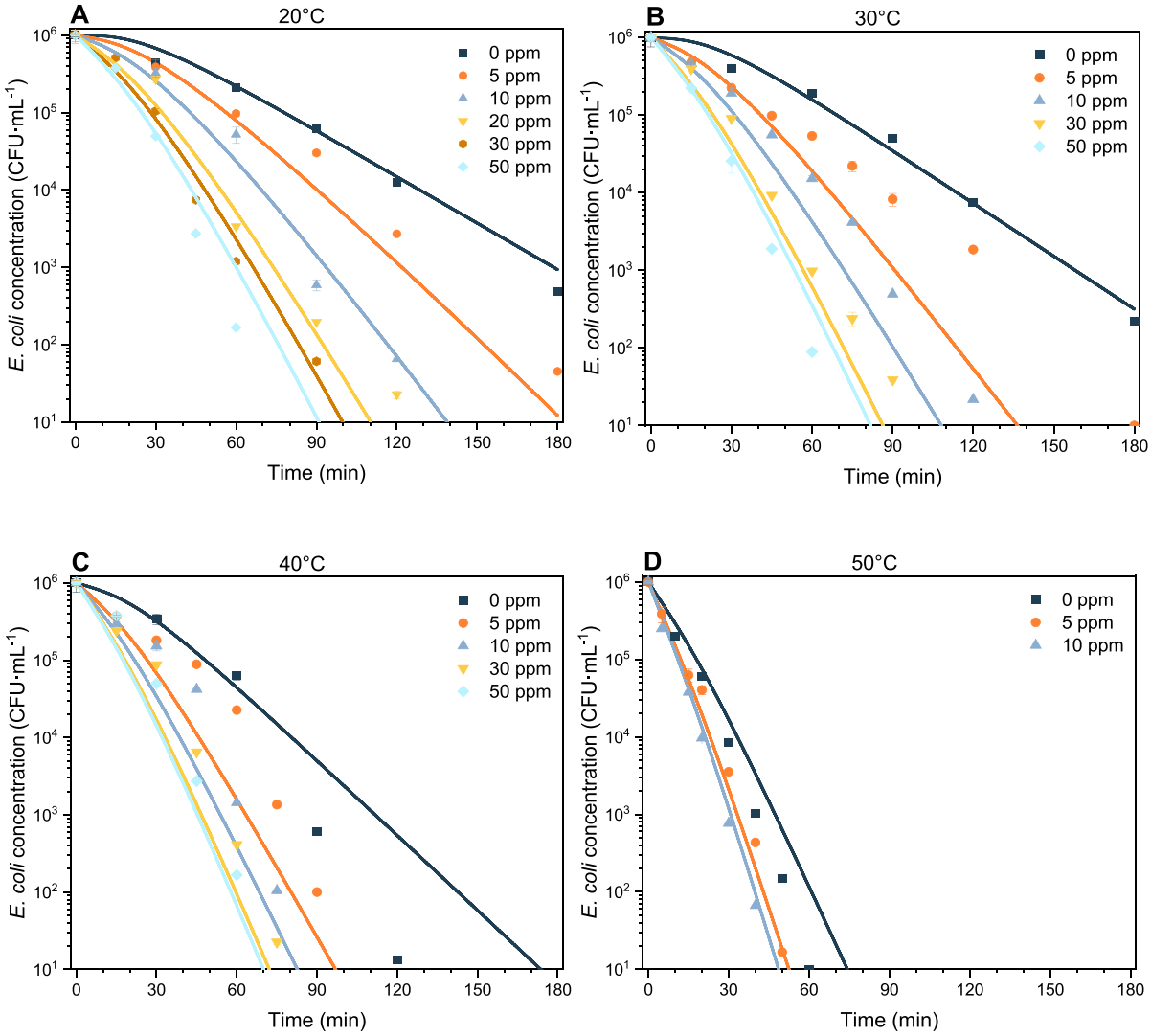

Fig. 3. Evolution of the *E. coli* concentration profiles depending on the initial H_2O_2 external concentration at different water temperatures. I = 15.0 W·m^{-2}. Line: predicted data. Dots: experimental data. A) 20 °C, B) 30 °C, C) 40 °C, and D) 50 °C.

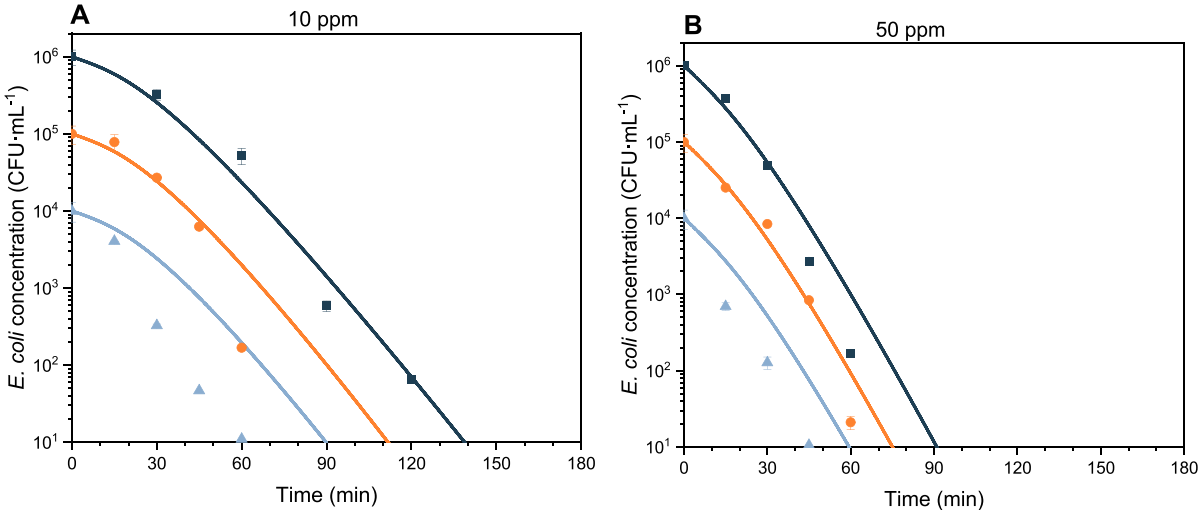

Fig. 4. Evolution of the *E. coli* concentration profiles depending on the initial cell concentration at different initial H_2O_2 external concentrations. I = 15.0 W·m^{-2}. Line: predicted data. Dots: experimental data. A) 10 ppm, B) 50 ppm.

4.3. T-UV Synergistic inactivation

The kinetic parameters of the synergy between UV radiation and temperature were estimated as $k_{016} = 4.16{\cdot}10^{-3}$ $m^2{\cdot}J^{-1}$, $Ea_{16} = 7.47{\cdot}10^3$ $J{\cdot}mol^{-1}$, with an NRMSLE of 14.0 %. The fitted curves are shown in Fig. 1, Fig. 2, and Fig. 3, as continuous lines. In Fig. 2, a saturation effect is observed when the external H_2O_2 concentration is increased above 10–20 ppm (10 ppm for 20–30 °C water temperature and 20 ppm for 40–50 °C). Two reasons cause this effect: the limitation of the H_2O_2 diffusion across the cell membrane is controlled by membrane permeation, and levels of internal H_2O_2 increase during solar illumination. Our model reproduces this behaviour with a high accuracy because of the incorporation of the H_2O_2 permeation into the cell (R.B), the overproduction of $O_2^{\bullet-}$ stimulated by solar light (R.12) and its subsequent conversion into H_2O_2 (R.2), as well as the deactivation of CAT (R.14). In spite of the SOD inactivation that also occurs (reducing the rate of H_2O_2 formation), the inactivation of CAT prevails ($k_{14} \gg k_{13}$), reducing the H_2O_2 conversion and inadvertently increasing the H_2O_2 levels inside the cell.

Due to the imposition given by eq. (5), the predictions done at 20 °C are the same for the synergistic and non-synergistic model. The value of the activation energy is not very high ($Ea_{SYN} = 7.47{\cdot}10^3$ $J{\cdot}mol^{-1}$) which involved a value of k_{16} only 1.33 times higher at 50 °C than at 20 °C. In contrast, the activation energy for the bacterial thermal inactivation resulted in being higher ($Ea_{11} = 1.38{\cdot}10^5$ $J{\cdot}mol^{-1}$) which implied a value of k_{11} almost 200 times higher at 50 °C than at 20 °C. Furthermore, the T-UV synergistic effect has also been observed for MS2 viruses and *Cryptosporidium parvum* protozoa whose activation energies were estimated to be three orders of magnitude higher (10^6) [56,57]. Hence, the synergistic effect is not very significant for this specific bacterial strain and experimental conditions. It is well known that, depending on the strain, bacteria can be more or less resistant to photoinactivation, radical damage, or even temperature effects [5]. However, it is also well known that the T-UV synergistic effect is usually common in the inactivation of microorganisms [25,56,57]. Since this model should be optimised for each type of strain, we have decided to include the description of the synergy, allowing the possibility of considering this effect.

4.4. Effect of operational conditions on disinfection rate

The modelling of the effect of UV solar light, water temperature, and concentration of H_2O_2 on the *E. coli* inactivation has been described and validated with experimental results hereabove. This mechanistic kinetic model allows elucidating the best operational conditions for the process. To this aim, the required solar exposure time to achieve a 99.99% of *E. coli* removal ($t_{99.99\%}$) has been obtained from the model's predictions. The combination of three water temperatures (20, 40, and 50 °C), three H_2O_2 concentrations (0, 10, and 50 ppm) and three UV irradiances (0, 15.0, and 20.8 $W{\cdot}m^{-2}$) constitute the operational conditions studied for this purpose. Fig. 5 shows the comparison of the $t_{99.99\%}$ for each scenario.

It can be seen that temperatures above 50 °C have a strong effect on bacterial inactivation whereas the thermal effect at 20–30 °C is negligible (here, only data at 20 °C is shown, but, as was concluded in Part 1, bacteria follow the same trend at 30 °C). For all the scenarios at 50 °C, times lower than 90 min were required to achieve the 99.99% of removal, being lower than 60 min when H_2O_2 was presented in the

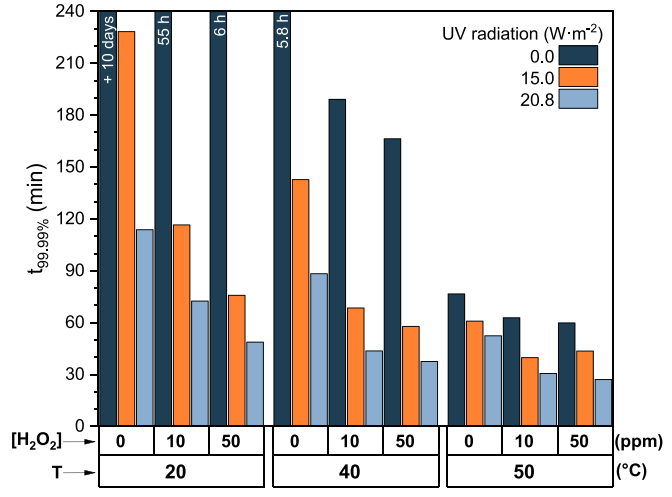

Fig. 5. Predictions of the required solar exposure time to achieve 99.99% of bacteria removal for different operational conditions of water temperature, external H_2O_2 concentration, and UV solar illumination.

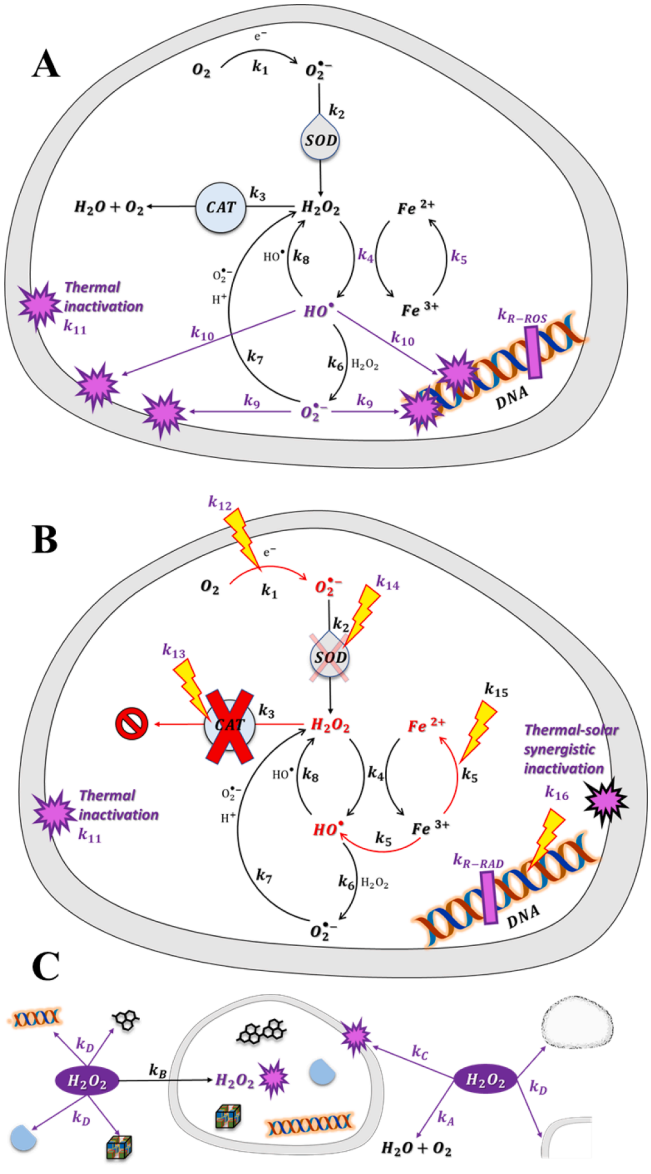

Fig. 6. Integrated mechanistic proposal for E. coli inactivation under the H_2O_2-enhanced inactivation process. A) Events taking place in the dark. B) Light-assisted events. C) Macroscopic and matrix-related events. Purple colour indicates the new kinetic constants and events contributed by this bi-partite work, and red shows the modifications inflicted by solar light. (For interpretation of the references to colour in this figure legend, the reader is referred to the web version of this article.)

water matrix or sunlight was provided.

If the thermal effect is not present (scenarios at 20 °C), the illumination with solar light is necessary in order to achieve inactivation times lower than 4 h (240 min). Even the addition of the higher H_2O_2 concentration (50 ppm) is not enough to require less than 6 h. Furthermore, if UV illumination and H_2O_2 addition are combined, the disinfection can be achieved in 50–120 min, and if the highest UV illumination or H_2O_2 dose (20.8 $W{\cdot}m^{-2}$ and 50 ppm) is used, the required time (50–90 min.) is comparable to the required times at 50 °C.

At 40 °C, the thermal effect contributes in the same way as the radiation and H_2O_2. In this case, the use of both variables simultaneously (UV illumination and H_2O_2 addition) in any of its studied values, result in required time between 50 and 90 min, analogous to required times at 50 °C.

As a conclusion, carrying out SODIS experiments at 50 °C of water temperature or at 20.8 $W{\cdot}m^{-2}$ of UV solar radiation (except for 20 °C and 0 ppm) requires less than 90 min to achieve the 99.99% of *E. coli* removal·H_2O_2 doses of 10 and 50 ppm do not achieve it for itself, but its combination with photonic and thermal effects contributes, achieving the bacterial reduction in less than 60 min.

4.5. Integrated solar E. coli inactivation mechanism, enhanced by H_2O_2

Having suggested the actions that take place in the dark under peroxide addition in various temperatures, the corresponding actions and modification occurring under solar irradiation and the effect of bacterial co-presence in the matrix, based on our modelling results of Part 1 and 2, we suggest an integrated scheme describing the solar/H_2O_2 experiments. The different pathways are highlighted alongside their kinetics, differentiating the values from other studies/literature and the ones resulting from this bi-partite work. Thus, a general overview indicating our contribution to the overall understanding of the problem is hereby presented in Fig. 6 (for simplicity and readability, the references previously supporting the findings are not repeated anew):

a) **Actions taking place in the dark** (Fig. 6***A***): Respiration in *E. coli* (and most aerobic bacteria) takes place involving the circulation of electrons, which, transferred to O_2 molecules can lead to the generation of $O_2^{\bullet-}$ (k_1). Superoxide radical, being a reactive transient, is normally handled by the cytoplasmic and periplasmic superoxide dismutases (SOD), leading to the production of H_2O_2 (k_2). Hydrogen peroxide is a more "preferred" ROS, because it is less reactive and hence, its presence is less dangerous for cell viability. However, scavenging mechanisms exist for H_2O_2 as well; catalases (CAT) and (hydroxy)peroxidases (e.g., Ahp, Ccp) catalyse its decomposition (k_3). The over-accumulation of H_2O_2 could be catastrophic, since iron is metabolically essential and present in the cell, and whose reaction with H_2O_2 leads to the highly reactive and non-selective $HO^{\bullet}$ (k_4), the Fenton process, alongside the ferrous to ferric iron oxidation. Ferric iron has its importance, although catalytically less active since electron donors could reduce it (k_5) and it can participate in the Fenton process. Although $HO^{\bullet}$ is the most oxidative and reactive species generated in the cell, the coexistence of ROS leads to less efficient but equally potentially dangerous reactions for the cell. $HO^{\bullet}$ reaction with H_2O_2 leads to further $O_2^{\bullet-}$ generation (k_6), whose augmented presence may lead to recombination and further H_2O_2 generation (k_7); this, in turn, can fuel the Fenton process. Finally, the high generation of $HO^{\bullet}$ can also present self-consumption, where $HO^{\bullet}$ can recombine to H_2O_2 (k_8), which is not an entire waste, but surely deprives the direct efficacy of the Fenton process in favour of its longer persistence. It is made clear that $O_2^{\bullet-}$, although a mild reductant, is of key importance since it affects the generation of other ROS, but also, it can directly affect several targets in the cell, e.g., iron/sulfur clusters, DNA and others (k_9). Surely, $HO^{\bullet}$ are more important, since they can damage DNA, proteins, and other macromolecules (k_{10}), but our results have indicated that similar steady-state concentrations may be achieved in the cell. Finally, we have identified and quantified the contribution of temperature in cell inactivation (k_{11}), a key aspect when H_2O_2 is added under solar light on in its absence. We should note here, that in our approach, we modelled the cell defences in a single process for simplification reasons ($k_{R\text{-}ROS}$), amassing the repair mechanisms against the intracellular oxidative stress at an appreciable rate compared to other processes.

b) **Actions modified under solar light** (Fig. 6***B****, actions that were presented in the dark are not repeated anew*): Solar light was found to accelerate electron dumping, which results in a significant increase in intracellular $O_2^{\bullet-}$ concentration (k_{12}). However, the most important change light inflicts to the system is the inactivation of CAT (k_{14}), which hampers its capacity to self-regulate H_2O_2. The corresponding light-mediated SOD inactivation was found to be significantly lower, which means that the higher $O_2^{\bullet-}$ generation may lead to higher H_2O_2 generation due to dismutation from SOD, as its functions are not severely impaired (k_{13}). These two effects lead to H_2O_2 over-accumulation and expose the cell to the risks of a higher Fenton process manifestation, with subsequent higher $HO^{\bullet}$ generation. In addition, a new pathway of $HO^{\bullet}$ generation is generated; the photo-Fenton process (k_{15}). This pathway consists of the light-assisted ferric-to-ferrous reduction, which sustains the Fenton process, as well as the additional generation of $HO^{\bullet}$, further contributing to cell lethality. Furthermore, we have measured the direct cell inactivation due to solar light (DNA damages, k_{16} in R.16–1), since DNA can absorb UVB light, and be damaged significantly. Nevertheless, in the presence of light, the effect of temperature is higher, influenced by the effect of photons, presenting a considerable synergy (k_{16} in R.16–2) that leads to cell inactivation in higher rates than light or heat alone. Last but not least, our modelling approach has measured the sum of the photo-induced responses to oxidative stress that may repair the cell alleviating the damages caused under light ($k_{R\text{-}RAD}$) in rates that are low but significant for cell survival.

c) **Macroscopic effects of H_2O_2/heat** (Fig. 6***C***): From the description of the dark events, it is made clear that H_2O_2 undergoes a spontaneous intracellular generation, while in water treatment under light (SODIS), an enhanced generation is expected. Nevertheless, in either case, H_2O_2 possesses a key role in the generation of $HO^{\bullet}$, with well-defined contributions. If H_2O_2 is added to the water, its role is dual, internally, and externally, in the bulk. Firstly, since during SODIS water temperature may rise, its self-decomposition was considered (k_A), before attributing a role to damages. These damages include the intracellular ones, mediated after its permeation into the cell (k_B), which shift the kinetics of the reactions that involve H_2O_2, such as the Fenton reaction, and the saturation of CAT scavenging capacity. As far as the extracellular damages are concerned, although of low oxidation potential (1.4 eV), multiple sites for reaction with the cell membrane (k_C) are considered, which can permit an effect in viability. Although not performed in our tests, it is expected that in high H_2O_2 concentrations, on the upper *mode-one/*low *mode-two killing* mechanisms levels, the thermodynamic limitations of H_2O_2 would be overcome by its high concentrations (kinetic influence), and may lead to an increased externally driven bacterial inactivation. Finally, our work contributed to the phenomenological aspects of cell–cell and cell-debris interaction in the water matrix (k_D), when it comes to H_2O_2 presence; inactivated cells and/or their fragments still play the role of H_2O_2 sinks, since they possess matter with which H_2O_2 can react. We estimated relatively high rates of reaction, which cannot be ignored. Under this scope, the solar/H_2O_2 treatment peroxide concentration profiles are explained, as to where the apparent H_2O_2 consumption is attributed to, improving the understanding of dynamically changing events taking place during SODIS/H_2O_2 water treatment.

4.6. Application of the model

The developed model allows the prediction of *E. coli* inactivation in clear water under sunlight with or without presence of H_2O_2. However, application in the field of SODIS processes may require further adaptations of the model and recalculation of the kinetic parameters to consider the actual conditions of the treatment.

First of all, if the process is conducted in closed recipients, the material may affect the radiation spectrum that reaches the water [59]. For instance, polyethylene terephthalate (PET) does not transmit UVB radiation, whereas other materials based on polypropylene (PP) and polymethylmethacrylate (PMMA) can be completely transparent to UVB. The absorption spectrum of DNA also comprises solar UVB radiation [60], and therefore, UVB is responsible for direct damage (R.16). Consequently, if PET is used, this specific reaction must be neglected. In contrast, absorption spectra of NADH [46], CAT [48], SOD [48], and iron [44] do comprise UVA radiation, so, these photoreactions (R.12, R.13, R.14, and R.15) should remain.

The presence in water of naturally occurring substances can also affect the kinetics of the SODIS process [61]. Optically active species, such as solid particles or humic acids, may act as radiation attenuators. Consequently, the incident radiation actually reaching the pathogens must be recalculated, especially in large volume containers. But they can also act as sensitisers, enhancing the kinetics of the process, such as, for instance, the presence of small concentrations of iron.

Finally, if the target indicator microorganism is different from the *E. coli* strain used in this work, the values of some of the kinetic parameters may require recalculation, especially those related to cell resistance, such as thermal inactivation (R.11:k_{011}, E_{a11}) bacterial damage by radicals (R.9: k_9, R.10: k_9, and k_{R-ROS}) and direct DNA damage + T-UV synergy (R.16:k_{016}, E_{a16} and k_{R-RAD}). In some cases, the mechanistic pathways of the inactivation may be revised, adding or removing specific reactions to describe oxidant scavenging enzymes or repair mechanisms.

5. Conclusions

The model presented in this work is the first approach to describe the main reactions of the *E. coli* inactivation by the SODIS process enhanced with H_2O_2 addition. The model successfully reproduced the experimental data of solar disinfection for different irradiances, water temperature and H_2O_2 concentration values (error = 14%). To describe the complex light/heat/H_2O_2 -mediated events, as well as for the accumulation of damage caused by radicals developed in the model under dark conditions, a new series-event model was developed; this model of the direct photonic inactivation is based on the accumulation of damage on DNA by photons and the rest of the events that get affected by light. A *multiple target - multiple hit* model was used to couple the two series-event models, also accounting for different recovery rates for each process (dark/light). As far as the thermal inactivation in the dark is concerned, the Arrhenius equation was incorporated in the kinetic constant of direct damage to account for the synergistic effect between solar radiation and temperature. Hence in overall, this kinetic model not only considers the photo-Fenton internal reaction, deactivation of enzymes and overproduction of radicals due to solar illumination, the dark events, the light/heat synergy, it also accounts for the sinks and macroscopic-level interactions of H_2O_2, producing an accurate phenomenological description.

A strength of the present mechanistic model is the capability of estimating inactivation profiles at different conditions of solar irradiance, water temperature and H_2O_2 concentration in the water matrix. However, the present venture is far from complete, but opens important new aspects for further research. For instance, it is recommended to optimise the kinetic parameters for other Gram-Negative bacterial strains for its proper generalisation before assessing the structurally different Gram-positive ones, and to further scrutinise high- H_2O_2 level experiments e.g. over 50 ppm of external H_2O_2 concentrations, to assess the possible contribution of *mode-two killing* that damages cell macromolecules and can provide new routes of cell inactivation.

Declaration of Competing Interest

The authors declare that they have no known competing financial interests or personal relationships that could have appeared to influence the work reported in this paper.

Acknowledgements

The authors acknowledge the financial support of the European Union's Horizon 2020 research and innovation programme in the frame of the PANIWATER project (GA 820718), funded jointly by the European Commission and Department of Science and Technology, India, and the Spanish State Research Agency (AEI) and the Spanish Ministry of Science, Innovation and Universities through the project CALYPSOL-ATECWATER (RTI2018-097997-B-C33). Stefanos Giannakis acknowledges the Spanish Ministry of Science, Innovation and Universities for the Ramón y Cajal Fellowship (RYC2018-024033-I). Ángela García Gil also acknowledges the Spanish Ministry of Education for her FPU grant (FPU17/04333). Ling Feng acknowledges the Natural Science Foundation of China (No. 42067032), and the China Scholarship Council (CSC: 201708155010).

References

[1] M.I. Polo-López, A. Martínez-García, M.J. Abeledo-Lameiro, H. H. Gómez-Couso, E. E. Ares-Mazás, A. Reboredo-Fernández, T.D. Morse, L. Buck, K. Lungu, K. G. McGuigan, P. Fernández-Ibáñez, Microbiological evaluation of 5 L- and 20 L-transparent polypropylene buckets for Solar Water Disinfection (SODIS), Molecules. 24 (11) (2019) 2193.

[2] Á. García-Gil, R.A. García-Muñoz, K.G. McGuigan, J. Marugán, Solar Water Disinfection to produce safe drinking water: A review of parameters, enhancements, and modelling approaches to make SODIS faster and safer, Molecules. 26 (2021) 3431, https://doi.org/10.3390/molecules26113431.

[3] E. Rommozzi, S. Giannakis, R. Giovannetti, D. Vione, C. Pulgarin, Detrimental vs. beneficial influence of ions during solar (SODIS) and photo-Fenton disinfection of *E. coli* in water: (Bi)carbonate, chloride, nitrate and nitrite effects, Appl. Catal. B Environ. 270 (2020) 118877.

[4] S. Giannakis, M.I. Polo-López, D. Spuhler, J.A. Sánchez Pérez, P. Fernández-Ibáñez, C. Pulgarín, Solar disinfection is an augmentable, in situ-generated photo-Fenton reaction—Part 1: A review of the mechanisms and the fundamental aspects of the process, Appl. Catal. B Environ. (2016) 199–223, https://doi.org/10.1016/J.APCATB.2016.06.009.

[5] K.L. Nelson, A.B. Boehm, R.J. Davies-Colley, M.C. Dodd, T. Kohn, K.G. Linden, Y. Liu, P.A. Maraccini, K. McNeill, W.A. Mitch, T.H. Nguyen, K.M. Parker, R. A. Rodriguez, L.M. Sassoubre, A.I. Silverman, K.R. Wigginton, R.G. Zepp, Sunlight-mediated inactivation of health-relevant microorganisms in water: a review of mechanisms and modeling approaches, Environ. Sci. Process. Impacts. 20 (2018) 1089–1122, https://doi.org/10.1039/c8em00047f.

[6] R.P. Sinha, D.-P. Häder, UV-induced DNA damage and repair: a review, Photochem. Photobiol. Sci. 1 (2002) 225–236, https://doi.org/10.1039/b201230h.

[7] R. Mosteo, A. Varon Lopez, D. Muzard, N. Benitez, S. Giannakis, C. Pulgarin, Visible light plays a significant role during bacterial inactivation by the photo-fenton process, even at sub-critical light intensities, Water Res. 174 (2020), 115636, https://doi.org/10.1016/j.watres.2020.115636.

[8] J. Jagger, Solar-UV actions on living cells, Praeger, 1985.

[9] M. Hessling, B. Spellerberg, K. Hoenes, W. Kneifel, Photoinactivation of bacteria by endogenous photosensitizers and exposure to visible light of different wavelengths - A review on existing data, FEMS Microbiol. Lett. 364 (2) (2017) fnw270.

[10] G.P. Pfeifer, Y.-H. You, A. Besaratinia, Mutations induced by ultraviolet light, Mutat. Res. Mol. Mech. Mutagen. 571 (2005) 19–31, https://doi.org/10.1016/j.mrfmmm.2004.06.057.

[11] L. Feng, C. Peillex-Delphe, C. Lü, D. Wang, S. Giannakis, C. Pulgarin, Employing bacterial mutations for the elucidation of photo-Fenton disinfection: Focus on the intracellular and extracellular inactivation mechanisms induced by UVA and H_2O_2, Water Res. 182 (2020), 116049.

[12] M. Castro-Alférez, M.I. Polo-López, P. Fernández-Ibáñez, Intracellular mechanisms of solar water disinfection, Sci. Rep. 6 (2016) 38145, https://doi.org/10.1038/srep38145.

[13] S. Chen, P. Schopfer, Hydroxyl-radical production in physiological reactions, Eur. J. Biochem. 260 (1999) 726–735, https://doi.org/10.1046/j.1432-1327.1999.00199.x.

[14] S. Giannakis, E. Darakas, A. Escalas-Cañellas, C. Pulgarin, Solar disinfection modeling and post-irradiation response of *Escherichia coli* in wastewater, Chem. Eng. J. 281 (2015) 588–598, https://doi.org/10.1016/j.cej.2015.06.077.

[15] S. Giannakis, S. Watts, S. Rtimi, C. Pulgarin, Solar light and the photo-Fenton process against antibiotic resistant bacteria in wastewater: A kinetic study with a Streptomycin-resistant strain, Catal. Today. 313 (2018) 86–93, https://doi.org/10.1016/j.cattod.2017.10.033.

[16] J. Moreno-Andrés, A. Acevedo-Merino, E. Nebot, Study of marine bacteria inactivation by photochemical processes: disinfection kinetics and growth modeling after treatment, Environ. Sci. Pollut. Res. Int. 25 (2018) 27693–27703, https://doi.org/10.1007/s11356-017-1185-6.

[17] M. Wang, M. Ateia, D. Awfa, C. Yoshimura, Regrowth of bacteria after light-based disinfection — What we know and where we go from here, Chemosphere. 268 (2021), 128850, https://doi.org/10.1016/j.chemosphere.2020.128850.

[18] S. Giannakis, A.I. Merino Gamo, E. Darakas, A. Escalas-Cañellas, C. Pulgarin, Monitoring the post-irradiation *E. coli* survival patterns in environmental water matrices: Implications in handling solar disinfected wastewater, Chem. Eng. J. (2014) 366–376, https://doi.org/10.1016/j.cej.2014.05.092.

[19] S. Gelover, L.A. Gómez, K. Reyes, M. Teresa Leal, A practical demonstration of water disinfection using TiO_2 films and sunlight, Water Res. 40 (2006) 3274–3280, https://doi.org/10.1016/j.watres.2006.07.006.

[20] A.-G. Rincón, C. Pulgarin, Absence of *E. coli* regrowth after Fe^{3+} and TiO_2 solar photoassisted disinfection of water in CPC solar photoreactor, Catal. Today. 124 (2007) 204–214, https://doi.org/10.1016/j.cattod.2007.03.039.

[21] P. Valero, S. Giannakis, R. Mosteo, M.P. Ormad, C. Pulgarin, Comparative effect of growth media on the monitoring of *E. coli* inactivation and regrowth after solar and photo-Fenton treatment, Chem. Eng. J. 313 (2017) 109–120, https://doi.org/10.1016/j.cej.2016.11.126.

[22] J. Ndounla, D. Spuhler, S. Kenfack, J. Wéthé, C. Pulgarin, Inactivation by solar photo-Fenton in pet bottles of wild enteric bacteria of natural well water: Absence of re-growth after one week of subsequent storage, Appl. Catal. B Environ. 129 (2013) 309–317, https://doi.org/10.1016/j.apcatb.2012.09.016.

[23] S. Shekoohiyan, S. Rtimi, G. Moussavi, S. Giannakis, C. Pulgarin, Enhancing solar disinfection of water in PET bottles by optimized in-situ formation of iron oxide films. From heterogeneous to homogeneous action modes with H_2O_2 vs. O_2 – Part 1: Iron salts as oxide precursors, Chem. Eng. J. 358 (2019) 211–224, https://doi.org/10.1016/j.cej.2018.09.219.

[24] J.A. Imlay, S. Linn, Bimodal pattern of killing of DNA-repair-defective or anoxically grown *Escherichia coli* by hydrogen peroxide, J. Bacteriol. 166 (1986) 519–527, https://doi.org/10.1128/jb.166.2.519-527.1986.

[25] K.G. McGuigan, R.M. Conroy, H.-J. Mosler, M. du Preez, E. Ubomba-Jaswa, P. Fernandez-Ibañez, Solar water disinfection (SODIS): A review from bench-top to roof-top, J. Hazard. Mater. 235 (2012) 29–46, https://doi.org/10.1016/j.jhazmat.2012.07.053.

[26] M. Castro-Alférez, M. Inmaculada Polo-López, J. Marugán, P. Fernández-Ibáñez, Validation of a solar-thermal water disinfection model for *Escherichia coli* inactivation in pilot scale solar reactors and real conditions, Chem. Eng. J. 331 (2018) 831–840, https://doi.org/10.1016/j.cej.2017.09.015.

[27] M. Castro-Alférez, M.I. Polo-López, J. Marugán, P. Fernández-Ibáñez, Mechanistic modeling of UV and mild-heat synergistic effect on solar water disinfection, Chem. Eng. J. 316 (2017) 111–120, https://doi.org/10.1016/j.cej.2017.01.026.

[28] S. Giannakis, E. Darakas, A. Escalas-Cañellas, C. Pulgarin, Temperature-dependent change of light dose effects on *E. coli* inactivation during simulated solar treatment of secondary effluent, Chem. Eng. Sci. 126 (2015) 483–487.

[29] S. Giannakis, E. Darakas, A. Escalas-Cañellas, C. Pulgarin, Elucidating bacterial regrowth: Effect of disinfection conditions in dark storage of solar treated secondary effluent, J. Photochem. Photobiol. A Chem. 290 (2014) 43–53, https://doi.org/10.1016/j.jphotochem.2014.05.016.

[30] S. Giannakis, E. Darakas, A. Escalas-Cañellas, C. Pulgarin, The antagonistic and synergistic effects of temperature during solar disinfection of synthetic secondary effluent, J. Photochem. Photobiol. A Chem. 280 (2014) 14–26.

[31] L. Uhl, A. Gerstel, M. Chabalier, S. Dukan, Hydrogen peroxide induced cell death: One or two modes of action? Heliyon. 1 (4) (2015) e00049.

[32] J. Moreno-SanSegundo, S. Giannakis, S. Samoili, G. Farinelli, K.G. McGuigan, C. Pulgarin, J. Marugán, SODIS potential: a novel parameter to assess the suitability of solar water disinfection worldwide, Chem. Eng. J. 419 (2021), 129889, https://doi.org/10.1016/j.cej.2021.129889.

[33] M.B. Fisher, M. Iriarte, K.L. Nelson, Solar water disinfection (SODIS) of *Escherichia coli, Enterococcus spp.*, and MS2 coliphage: Effects of additives and alternative container materials, Water Res. 46 (2012) 1745–1754, https://doi.org/10.1016/j.watres.2011.12.048.

[34] M. Castro-Alférez, M.I. Polo-López, J. Marugán, P. Fernández-Ibáñez, Mechanistic model of the *Escherichia coli* inactivation by solar disinfection based on the photo-generation of internal ROS and the photo-inactivation of enzymes: CAT and SOD, Chem. Eng. J. 318 (2017) 214–223, https://doi.org/10.1016/j.cej.2016.06.093.

[35] W.H.O. World Health Organization, WHO International Scheme to Evaluate Household Water Treatment Technologies Harmonized Testing Protocol: Technology Non-Specific., 2014.

[36] M. Marjanovic, S. Giannakis, D. Grandjean, L.F. de Alencastro, C. Pulgarin, Effect of μM Fe addition, mild heat and solar UV on sulfate radical-mediated inactivation of bacteria, viruses, and micropollutant degradation in water, Water Res. 140 (2018) 220–231, https://doi.org/10.1016/j.watres.2018.04.054.

[37] SUNTEST CPS/CPS+ (1999) 32.

[38] J. Rodríguez-Chueca, S. Giannakis, M. Marjanovic, M. Kohantorabi, M.R. Gholami, D. Grandjean, L.F. de Alencastro, C. Pulgarín, Solar-assisted bacterial disinfection and removal of contaminants of emerging concern by Fe^{2+}-activated HSO_5- vs. $S_2O_8^{2-}$ in drinking water, Appl. Catal. B Environ. (2019) 62–72.

[39] J.A. Imlay, I. Fridovich, Assay of metabolic superoxide production in *Escherichia coli*, J. Biol. Chem. 266 (11) (1991) 6957–6965.

[40] J. Zheng, J.F. Domsic, D. Cabelli, R. McKenna, D.N. Silverman, Structural and kinetic study of differences between human and *Escherichia coli* Manganese Superoxide Dismutases, Biochemistry. 46 (2007) 14830–14837, https://doi.org/10.1021/bi7014103.

[41] G.V. Buxton, C.L. Greenstock, W.P. Helman, A.B. Ross, Critical Review of rate constants for reactions of hydrated electrons, hydrogen atoms and hydroxyl radicals (·OH/·O⁻ in Aqueous Solution, J. Phys. Chem. Ref. Data. 17 (1988) 513–886, https://doi.org/10.1063/1.555805.

[42] H. Gallard, J. De Laat, Kinetic modelling of Fe(III)/H_2O_2 oxidation reactions in dilute aqueous solution using atrazine as a model organic compound, Water Res. 34 (2000) 3107–3116, https://doi.org/10.1016/S0043-1354(00)00074-9.

[43] G.V. Buxton, A.J. Elliot, Temperature dependence of the rate constant for the reaction H + OH in liquid water up to 200 °C, J. Chem. Soc. Faraday Trans. 89 (1993) 485–488, https://doi.org/10.1039/FT9938900485.

[44] C. Casado, J. Moreno-SanSegundo, I. De la Obra, B. Esteban García, J.A. Sánchez Pérez, J. Marugán, Mechanistic modelling of wastewater disinfection by the photo-Fenton process at circumneutral pH, Chem. Eng. J. 403 (2021), 126335, https://doi.org/10.1016/j.cej.2020.126335.

[45] L.C. Seaver, J.A. Imlay, Hydrogen peroxide fluxes and compartmentalization inside growing *Escherichia coli*, J. Bacteriol. 183 (2001) 7182–7189, https://doi.org/10.1128/JB.183.24.7182-7189.2001.

[46] M. Tanaka, K. Ohkubo, S. Fukuzumi, DNA cleavage by UVA irradiation of NADH with dioxygen via radical chain processes, J. Phys. Chem. A. 110 (2006) 11214–11218, https://doi.org/10.1021/jp064130r.

[47] Y. Hakamada, K. Koike, T. Kobayashi, S. Ito, Purification and properties of mangano-superoxide dismutase from a strain of alkaliphilic Bacillus, Extremophiles. 1 (1997) 74–78, https://doi.org/10.1007/s007920050017.

[48] W.G. Dos Santos, I. Pacheco, M.Y. Liu, M. Teixeira, A.V. Xavier, J. LeGall, Purification and characterization of an iron superoxide dismutase and a catalase from the sulfate-reducing bacterium *Desulfovibrio gigas*, J. Bacteriol. 182 (2000) 796–804, https://doi.org/10.1128/JB.182.3.796-804.2000.

[49] J.E. Visick, S. Clarke, RpoS- and OxyR-independent induction of HPI catalase at stationary phase in *Escherichia coli* and identification of rpoS mutations in common laboratory strains, J. Bacteriol. 179 (1997) 4158–4163, https://doi.org/10.1128/jb.179.13.4158-4163.1997.

[50] H.P. Misra, I. Fridovich, Inhibition of superoxide dismutases by azide, Arch. Biochem. Biophys. 189 (1978) 317–322, https://doi.org/10.1016/0003-9861(78)90218-7.

[51] I. Fridovich, Superoxide dismutases, Annu. Rev. Biochem. 44 (1975) 147–159, https://doi.org/10.1146/annurev.bi.44.070175.001051.

[52] L.T. Benov, I. Fridovich, *Escherichia coli* expresses a copper-and zinc-containing superoxide dismutase, J. Biol. Chem. 269 (1994) 25310–25314, https://doi.org/10.1016/S0021-9258(18)47248-1.

[53] M.N. Chong, B. Jin, C.W.K. Chow, C. Saint, Recent developments in photocatalytic water treatment technology: A review, Water Res. 44 (2010) 2997–3027, https://doi.org/10.1016/j.watres.2010.02.039.

[54] M.M. Busse, M. Becker, B.M. Applegate, J.W. Camp, E.R. Blatchley, Responses of *Salmonella typhimurium* LT2, *Vibrio harveyi*, and *Cryptosporidium parvum* to UVB and UVA radiation, Chem. Eng. J. 371 (2019) 647–656.

[55] B.F. Severin, M.T. Suidan, R.S. Engelbrecht, Kinetic modeling of U.V. disinfection of water, Water Res. 17 (1982) 1669–1678, https://doi.org/10.1016/0043-1354(83)90027-1.

[56] Á. García-Gil, M.J. Abeledo-Lameiro, H. Gómez-Couso, J. Marugán, Kinetic modeling of the synergistic thermal and spectral actions on the inactivation of *Cryptosporidium parvum* in water by sunlight, Water Res. 185 (2020), 116226, https://doi.org/10.1016/j.watres.2020.116226.

[57] Á. García-Gil, A. Martinez, M.I. Polo-López, J. Marugán, Kinetic modeling of the synergistic thermal and spectral actions on the inactivation of viruses in water by sunlight, Water Res. 183 (2020), 116074, https://doi.org/10.1016/j.watres.2020.116074.

[58] H. Byun, E. Lee, D. Oh, S. Kim, M. Park, Denaturation and inactivation of antioxidative enzymes due to repeated exposure to UV-B and inhibitory effect of RGP lens, J. Korean Ophthalmic Opt. Soc. 20 (2015) 237–246, https://doi.org/10.14479/jkoos.2015.20.2.237.

[59] A. García-Gil, C. Pablos, R.A. García-Muñoz, K.G. McGuigan, J. Marugán, Material selection and prediction of solar irradiance in plastic devices for application of solar water disinfection (SODIS) to inactivate viruses, bacteria and protozoa, Sci. Total Environ. 730 (2020), 139126, https://doi.org/10.1016/j.scitotenv.2020.139126.

[60] Y. Jiexi, W. Kairong, D. Wen, C. Ru, X. Junqiu, Z. Bangzhi, S. Jingjing, W. Rui, Two hits are better than one: membrane-active and DNA binding-related double-action mechanism of NK-18, a novel antimicrobial peptide derived from mammalian NK-Lysin, Antimicrob. Agents Chemother. 57 (2013) 220–228, https://doi.org/10.1128/AAC.01619-12.

[61] Á. García-Gil, R. Valverde, R.A. García-Muñoz, K.G. McGuigan, J. Marugán, Solar Water Disinfection in high-volume containers: Are naturally occurring substances attenuating factors of radiation? Chem. Eng. J. 339 (2020), 125852 https://doi.org/10.1016/j.cej.2020.125852.